

Article

Exploring Neogene Marine Diatomites in Western Crete: A New Source-Rock Candidate with Hydrocarbon Generation Potential?

Dimosthenis Telemenis ¹, Vagia-Ioanna Makri ^{1,2} , Emmanouil Manoutsoglou ¹  and Spyridon Bellas ^{2,*} ¹ School of Mineral Resources Engineering, Technical University of Crete, 73100 Chania, Greece² Institute of GeoEnergy, Foundation for Research and Technology-Hellas (FORTH/IG), 73100 Chania, Greece

* Correspondence: spyrosbellas@ipr.forth.gr

Abstract: Diatomites are sedimentary rocks rich in siliceous algae, mainly diatoms, and are evident in Greece mainly in Neogene successions. Despite their significance and worldwide potential as source rocks for hydrocarbons, little is known about them in the wider area of Greece, limited in their biostratigraphic characteristics and industrial use. This study assesses for the first time the Neogene diatomites in Western Crete and focuses on their source rock quality and hydrocarbon generation potential on top of their stratigraphic characteristics. The studied synthetic outcrop is of the Miocene age and is located in the Apokoronas sedimentary basin, in the Chania province. It is subdivided into four subsections reaching heights of 13 m. It has a total documented, visible extend of 90–100 m and presents adequate thickness in relation to other reported diatomitic occurrences in Crete. A SEM study and bulk sampling of 28 samples has been carried out on this outcrop and geochemical analysis has been conducted by means of a Rock-Eval 6 pyrolysis to facilitate the understanding of hydrocarbon potential. Stratigraphic analysis supports the establishment of system tracts (ST), with transgressive ones (TST) illustrated by fining-upward sequences including highstands (HST). At the top, a final coarsening-upwards sequence suggests a regressive sequence (RST) most probably related to the Messinian Salinity Crisis (MSC) event. Total organic carbon (TOC, %wt.) values are found to reach 3.4% in the diatomites, while siltstone/mudstone interlayers encounter lower TOC (%wt.), yet with exceptions reaching TOC levels as high as the diatomaceous facies. Overall, Rock-Eval pyrolysis shows that organic matter from the studied cross sections is immature with the hydrocarbon generation potential ranging from poor to excellent. The kerogen type is proved to be type III with poor to almost good quality. This suggests the presence of a prolific diatomaceous source rock in Western Crete demonstrating a high significance for the offshore hydrocarbon exploration in the Eastern Mediterranean that could potentially be related to the offshore Western and Southern Crete E&P-awarded blocks.

Keywords: diatomites; hydrocarbons; organic geochemical analysis; source rock; Crete; Neogene; Miocene; stratigraphy; pre-evaporitic; eastern Mediterranean



Citation: Telemenis, D.; Makri, V.-I.; Manoutsoglou, E.; Bellas, S. Exploring Neogene Marine Diatomites in Western Crete: A New Source-Rock Candidate with Hydrocarbon Generation Potential? *Eng* **2023**, *4*, 285–300. <https://doi.org/10.3390/eng4010017>

Academic Editors: Reza Rezaee and Yujie Yuan

Received: 15 December 2022

Revised: 12 January 2023

Accepted: 16 January 2023

Published: 18 January 2023



Copyright: © 2023 by the authors. Licensee MDPI, Basel, Switzerland. This article is an open access article distributed under the terms and conditions of the Creative Commons Attribution (CC BY) license (<https://creativecommons.org/licenses/by/4.0/>).

1. Introduction

Diatomites are light, soft, easily powdered, fine-grained, consolidated, sedimentary rocks mostly composed of the siliceous frustules of diatoms, silicoflagellates, sponge spicules and/or radiolaria, well-organized in cyclic alternations (laminae) of light and dark color respectively, and usually connected to seasonal variability between winter and summer. Unconsolidated lake or marine deposits with no diagenesis may be called diatomaceous ooze [1]. They include both freshwater and marine habitats. Rich marine diatomaceous deposits, diatom blooms, are usually connected to the increased productivity of upwelling systems, perhaps the most well-known of them being the offshore area of Chile (i.e., [2]).

Diatomitic occurrences are widespread in the Mediterranean. One of the first distribution maps of Messinian laminated diatomaceous formations of the western Mediterranean was provided by [3] where the authors tried to connect them to the upwelling and high nutrient influx. [4] published a similar map for the entire Mediterranean siliceous deposits. Recently, thorough research of the parameters that govern the relationship between biogenic silica and organic matter (OM) preservation during the upper Miocene of northern Italy is given in [5].

Most publications refer to the diatomites either from a lithostratigraphic and biostratigraphic point of view, or as industrial material with variable usages, including environmental ones [6–9]. Among others, their significance relies on their high value in hydrocarbon exploration. The latter is supported mainly by their gas generation potential as suggested by several research works [10–12] as well as their prolific hydrocarbon source-rock character in many basins worldwide ([12–17]).

Diatomites have never been utilized as prolific source rocks for hydrocarbon Exploration and Production (E&P) in the Mediterranean Sea, despite the sector’s strong activation during the last two decades. In this context, the present work investigates diatomites outcropping in NW Crete, Greece (Figure 1). The first lithostratigraphic subdivision of western Crete (Chania Province) was introduced by [18]. According to this author, the presently studied siliceous deposits resemble the Italian “tripoli” and can be placed in the upper Miocene Khairithiana formation; compare also [19]. Messinian upwelling systems that resulted in diatomitic strata accumulation were reported from only four locations in Greece, three in Crete (see review in [20,21]) and one in the Gavdos Islands [22–24], while six in total are reported from the eastern Mediterranean (including one in Cyprus and one in Turkey respectively [25]). Thorough research on the upper Miocene strata of Crete geochemical signatures was recently published by [26], but no reference to diatomitic deposits is made therein.

This paper focuses on the geochemical study of a newly reported [27] thick occurrence of diatomitic laminites from the western Crete Island in Greece. An open system pyrolysis of the samples was applied by means of Rock-Eval 6 (RE6). Stratigraphic data are also provided for the better understanding of the geological connection to the prevailing paleodepositional environments. This approach aims to uncover the potential of the diatomites as a new source rock for hydrocarbon generation in Greece and broadly in the eastern Mediterranean Sea. In the recent context of energy supply deficiency in Europe and worldwide, such discoveries may provide the solution at least for the transition period to fully renewables development which will for sure last for the next two to three decades.

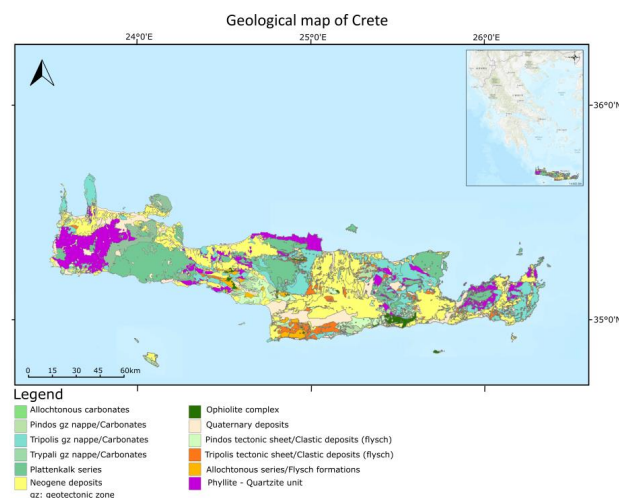


Figure 1. Geological map of Crete with the study outcrop indicated by a red box. Map modified after Decentralized Administration of Crete—IT and Communications Directorate (www.data.apdkritis.gov.gr, accessed on 11 November 2022) [28]. In yellow the main Neogene basins of Crete, bearing transgressive strata on the pre-Neogene basement.

2. Geological Setting

In the eastern Mediterranean Sea and particularly in Greece, a prominent geologic structure is the active collision of the European (Aegean microplate) and the African lithospheric plates. As the latter proceeds to the north, both the subduction and the roll-back effect contribute to a complex geodynamic regime, known as the Hellenic Arc and Trench System (HEAT) or the Hellenic Subduction Zone (HSZ), that is curvature-like and develops from the Adriatic/Ionian Seas to the northwest of Greece, down to the Crete Island to the south and further east to the Rhodes Island [29–32]. A number of mega-structures are directly related to this movement at the plate boundaries, namely the Aegean Volcanic Arc (i.e., Santorini volcanic island) to the north, an uplift (exhumation) resulting in the Crete island and subsequent neogene basin development [33], a backstop, the Mediterranean Ridge accretionary complex to the south [34] and deep offshore trenches mainly due to strike-slip accommodation to the west–southwest (e.g., Matapan) [35] and south–southeast of Crete (e.g., Pliny, Strabo and Ptolemy, [36,37]).

The modern situation of the Aegean, based mostly on offshore data, Plio-Quaternary Extension and strike-slip kinematics that led to the present structural framework was given by [38] and the references therein. Based on satellite-geodetic and earthquake analysis data a thorough reconstruction with two models for the past 1 and 5 Myr of the crustal rotation in the Aegean is recently provided by [39,40].

A structural fragmentation of the exhumed pre-Neogene basement (including mostly HP-LT metamorphic rocks) in multi-blocks led to the development of the Cretan basins, where late middle-to-upper Miocene and Pliocene clastic and carbonate sediments accumulated [41–43]. The initially N–S oriented extension was followed by the E–W extension in the course of Miocene, while the tilting of Crete to the N–NW prevailed in the Pliocene [33]. Beginning of subsidence and sedimentation is assigned an age of 10.8 Ma [44]. According to the later authors, an age of ~9.6 Ma may be attributed to the development of the present-day shape (horst-like) of Crete Island, although the rough relief today was largely shaped in the Pleistocene and Holocene [21]. Refs. [45,46] highlighted the Holocene paleoshoreline uplift of SW Crete due to normal faulting as a result of major earthquakes.

In western Crete and specifically in the Chania Province, the Neogene deposits present with a large geographical extension. Eleven (11) lithostratigraphic formations (Fms.) were recognized by [18], some of them passing laterally to one another. Two main Fms. groups were separated, based on the Gypsum presence stratigraphic level (documenting the Messinian Salinity Crisis evaporites, MSC). According to [18], these are the Ayios Georgios and Kissamou Fms. (below Gypsum), unconformably resting on the pre-Neogene, followed upwards by the Akrotiri, Khairethiana and Tavronitis Fms. (above Gypsum level). Following [33,41] in turn, there was a recognition of six (6) lithostratigraphic groups of Cretan formations. Four (4) of them belong to Miocene (Prina, Tefelion, Vrysses and Hellinikon groups) and two (Finikia and Aghia Galini groups) are of the Pliocene age.

All these lithostratigraphic schemes based on the facies differentiation assumption may clearly be the depositional result of two distinct and complete sedimentation cycles (transgression, highstand, regression), separated by the MSC regressional event; the first event of the Miocene age (lasting from the Tortonian to Messinian) and the second one of the Pliocene age (uppermost Zanclean to early Piacenzian) [20,47,48]. The later authors recognized a third sedimentation cycle as well, a Pleistocenic one, with terraces locally raised in some cases at 200 m altimeter as a result of the combination of high rates of tectonic uplift and enormous sea-level changes affecting various levels of existing deposits.

The diatomitic deposits that are presently studied represent a new occurrence of fine laminites in Crete [27]. The studied outcrop represents a synthetic one, subdivided into three main subsections. It is located in the Apokoronou District of Chania Prefecture, directly to the south of Soudha Bay, the main port of western Crete. It is widely (visibly) and linearly extended along the main street of Kalyves village in a west–east direction, but sparse occurrences of it can be followed up to at least 1 km away (to the west) of the main outcrop location. According to the map of [18] it is postulated that it belongs to

the Khairethiana Fm. Although the later author placed it in the Pliocene (above Gypsum level), this formation's deposits were later on assigned a Miocene age based on planktonic Foraminifera biostratigraphy [49], a fact which fits well with our observations.

3. Materials and Methods

3.1. Lithostratigraphic Logging, Sampling Procedure and Microscopy

As mentioned above, the studied material comes from a synthetic outcrop, where Miocene laminites are well exposed in the Kalyves village, Apokoronou District of Chania Prefecture. The methodology applied included field work for the identification of the specific rock type that we were interested in (i.e., diatomites), detailed section logging, combined with lateral equivalents in order to manage the strata continuity and appropriate sampling. Scanning Electron Microscopy (SEM) used on a set of samples to elaborate on the type (diatomites or not) and preservational status and structure of laminites.

Bulk sampling of twenty-eight (28) samples was carried out in three locations (Figure 2). It is an undisturbed profile, comprising a depositional sequence that measures more than a hundred meters in horizontal length and tens of meters in thickness. Layers are horizontally stratified, therefore following the lateral extension of it was not such a problem. The outcrop is subdivided into four (4) subsections, due to difficulties in access and sampling by heavy vegetation and steepness of it: the lower part, represented by subsections i and ia (twenty one (21) samples: 1, 1b to 9; plus the ex2 and 10 to 15), the intermediate part, represented by subsection b (three (3) samples: 20 to 22) and the upper part, subsection c (four (4) samples: 23 to 26). To control the lateral continuity, additional side sampling was undertaken as well (four (4) samples: 16 to 19). Sixteen (16) in total samples can be described as diatomites.



Figure 2. The studied synthetic outcrop in Kalyves village (west Crete, Greece, yellow arrow). Red boxes and relevant arrows point to the sampling route followed from the basal part of the profile (subsection i, ia; near shore), to the intermedium part of it (subsection b), and further to the top (subsection c; box to the right). The grey line crossing the map is the national road driving from Chania (to the left, or west) to Rethymnon city (to the right, east, light blue arrow).

SEM samples used both as raw rock material (rock fragments) and as processed samples. Six (6) samples in total were processed for SEM imaging, representing all four subsections of the studied outcrop (4, 8, 13, 21, 25) and a side one (16). Preparation included fragmentation of the rocks, treatment with light H_2O_2 (5%) for 24 h, and with deionized water for another day, followed by dispersion of the material onto the traditional SEM stubs and subjected to graphite coating procedure (film thickness of ~25 nm). Gold sputtering procedure applied only in one sample (2022-4-6-CK-2(16)-ITE). Microphotographs were kindly undertaken in the Jeol JSM-IT500 SEM of the Hellenic Authority for Geological and Mining Research, under beam voltage of 20 kV and in low vacuum of 30–50 Pa,

out of two samples that experimentally proceeded under ultra-high vacuum (samples 2022-4-6-CK-2(16)-ITE and 2022-4-6-CK-1(13)-ITE).

3.2. Rock Eval 6 Pyrolysis

Rock-Eval 6 (RE6) pyrolysis was performed on all the 28 outcrop samples using a Rock-Eval 6[®] anhydrous open-system pyrolyser (Vinci Technologies, France) [50]. The basic setup/bulk-rock method for the organic matter analysis [51,52] was applied to characterize the potential source rock samples and assess their hydrocarbon generation potential. The analysis provided measurements from the sequential pyrolysis and oxidation of ca. 50–60 mg of finely grounded (<250 µm) sample amount, according to [53]. The resulting volatile hydrocarbons from pyrolysis were detected and quantified using a flame ionization detector (FID) which was also used to quantify the CO and CO₂ gases resulting from both pyrolysis and oxidation. Pyrolysis followed an isothermal trend from 300 °C where it stayed for 3 min and a subsequent 25 °C/min ramp until 650 °C. Subsequently the oxidation was carried out from 300 to 850 °C with a heating rate of 20 °C/min [53].

Based on this analysis, the following parameters were determined; The free hydrocarbons in the sample from the intensity of the S1 peak (S1; mg hydrocarbon per g rock), the hydrocarbons formed by the thermal cracking of kerogen determined from the intensity of the S2 peak (S2, mg HC/g rock), the total organic carbon (TOC, %wt.), the temperature Tmax (°C) at which the maximum number of hydrocarbons is generated. On top of these, the carbon monoxide (CO) and carbon dioxide (CO₂) released during the thermal decomposition of OM (S3CO and S3CO₂ peaks) were also determined after pyrolysis and oxidation, along with the inorganic carbon content (pyroMINC and oxiMINC peaks).

4. Results

4.1. Lithostratigraphy

The lower subsections (i and ia) display the base of the whole outcrop (Figure 3). Section i is approximately 2.90 m thick, followed by section ia which accounts for 2.70 m. The lowermost part of section i was grey/blueish, thinly to medium bedded, locally bioturbated, fine sand-to-siltstones moderately cemented, and reached up to 1.80 m. The following-upwards part is 1.10 m consisting entirely of whitish, brittle, silty diatomites (Figure 3, right part –i-, lower yellow horizon), well organized in fine (thickly laminated to very thinly bedded) laminae alternations (varve-like). Section ia consists of similar alternations, wherein the bottom part (1.35 m) contains mostly silty mudstones and an underlying of 0.95 m of well-laminated (Figure 3, right upper part –ia- yellow horizon) white-to-slightly-light grey diatomaceous deposits. The section “closes” at the top via a 0.4 m thick sandstone layer, which is partly oxidized.

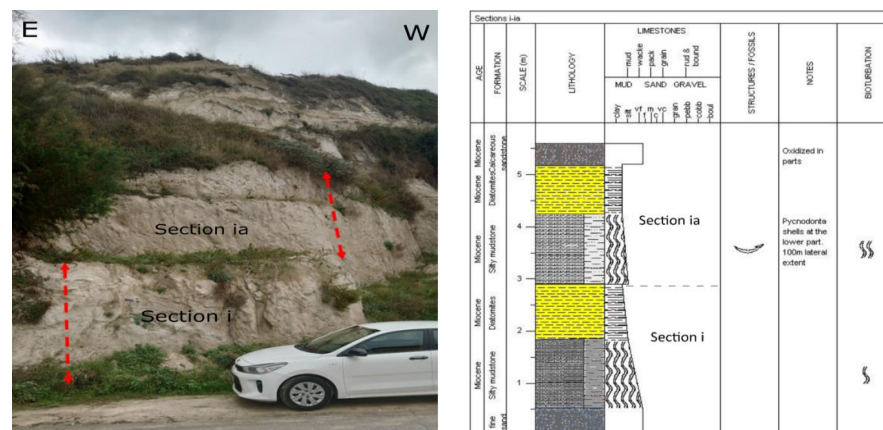


Figure 3. The lower (basal) part of the Kalyves synthetic outcrop. To the left is the field photograph of subsections i and ia, which are depicted with the red dashed lines. To the right is the profile logging. In yellow colour the laminated diatomite packages.

Section b (Figure 4) represents the middle package of diatomites and the upwards continuation of the lower part (sections i, ia). The whole profile falls inside a construction site, so unfortunately the available data will be lacking for future scientific work. The sampled sector is approximately three (3) meters thick, while the whole subsection has a thickness of about 7.60 m, extending a few meters further down but impossible to sample. A blueish-to-light grey silty mudstone comprises the bottom part, gradually followed upwards by pure, light, whitish, very friable diatomites (Figure 4, upper part in yellow). In one sample near the top, marine fish-fauna rests were found, but due to friability they were not possible to be identified, although this indicated that a deep marine paleoenvironment persisted in the area during the upper Miocene.

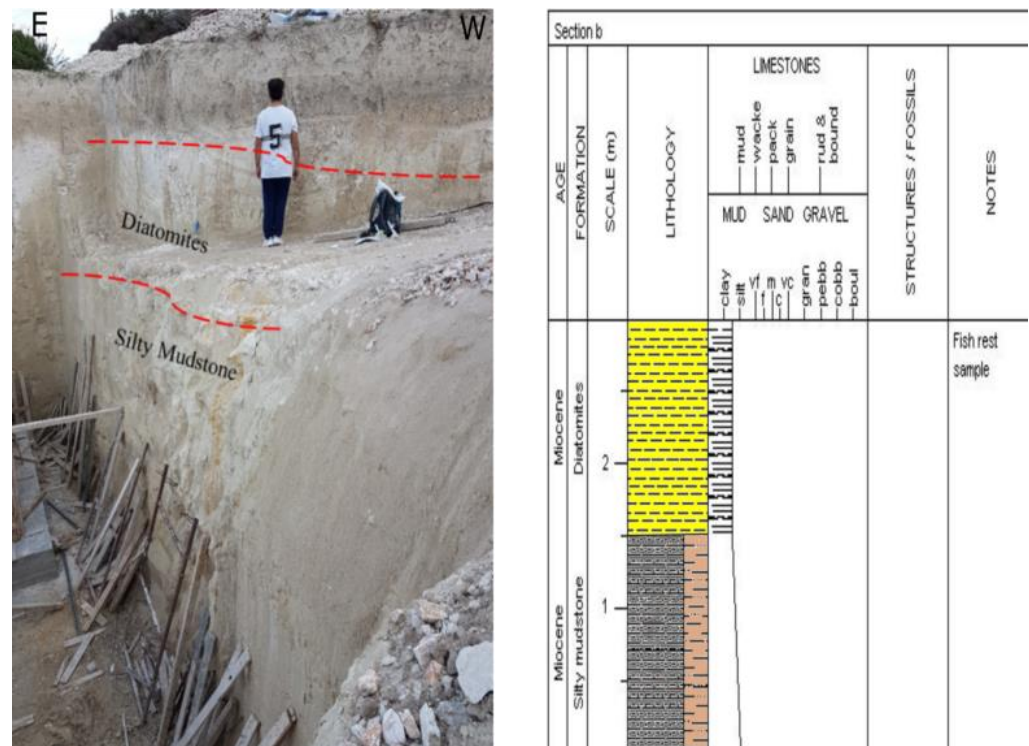


Figure 4. To the left, the construction site of studied subprofile b. Thinly-to-medium bedded silty mudstone at the base, passes gradually to the diatomitic laminites at the top (man for scale). To the right, the relevant lithostratigraphic log. In yellow color the diatomites.

Section c (Figure 5) represents the upper (top) package of silty mudstones and diatomites, comprising a total thickness of 3.60 m. In this part, yellowish silty mudstones underlie the diatomitic beds (Figure 5, middle part in yellow). The section closes at the top with three (3) medium-to-thickly bedded, indurated sandy mudstone beds, showing signs of oxidation and representing the closure of the studied synthetic outcrop whilst being covered by recent soil, bearing a root system of natural plants. A rapid uplift probably occurred in the area with subsequent erosion that did not enable the deposition of a normal regressive sequence to be developed.

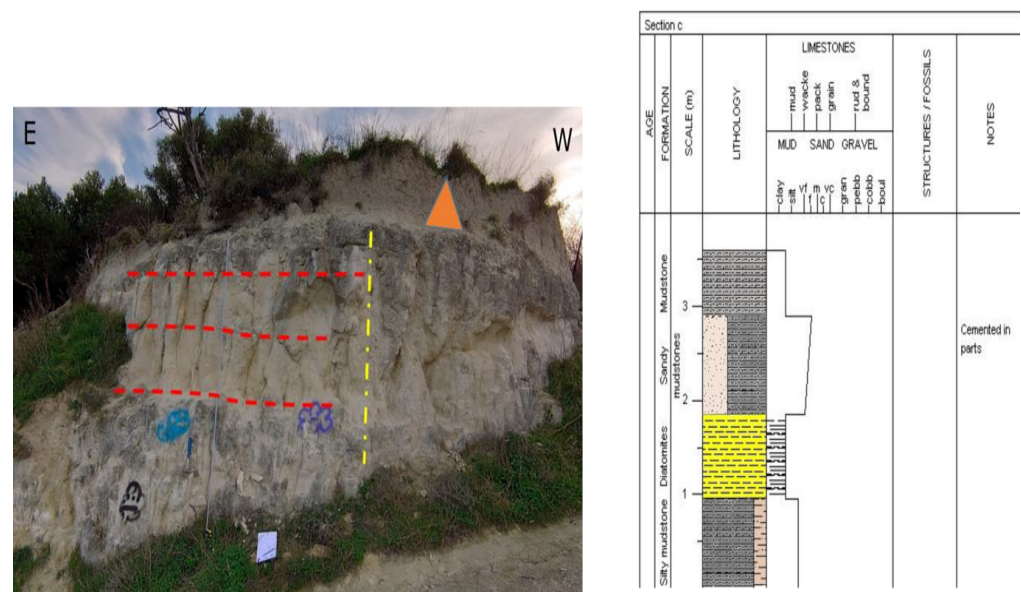


Figure 5. To the left is the topmost subsection of the studied synthetic outcrop of diatomites. The dashed red lines depict the sandy mudstone beds overlying the diatomitic horizons. Geological hammer for scale. To the right the subsection lithostratigraphic logging with the diatomites in yellow.

4.2. Sequence Stratigraphy

For a comprehensive review and standardization of the sequence stratigraphy methodology, the reader is referred to [54] and the references therein. The total synthetic outcrop currently studied is a depositional package belonging to the first Neogene sedimentation cycle of western Crete according to [20,41,47,48] of the Upper Miocene age. Between the basal part of it (subsection i) and the top (Section c), a cycling of deepening-to-shallowing strata is observed. The lower part of the subsection i (Figure 3) represents a transgressive, deepening deposit (TST), probably as a response to changes in the accommodation space (as a result of both the tectonic subsidence of north Cretan subbasins and sea-level rise). The absolute base of it is not visible, since no pre-Neogene basement occurs in the close neighborhood, therefore no real sequence boundary (unconformity) can be drawn. The diatomite strata that follow the up section consisting of fine, varve-like laminae seem to reflect an extra deepening, indicating a more distal setting than the lower part [55,56]. Similar siliceous sedimentary facies are usually attributed to basinal facies [57]. As the SEM study provided, the diatoms are dominated by circular forms (Figure 6), thus supporting the distal setting of deposition. Subsection ia (Figure 3, upper part) is lithostratigraphically a repeat of i, indicating firstly a slight shallowing (relative sea-level fall) followed again by a deepening and highstand, documented by the upper diatomites deposition (Figure 3, in yellow; Figure 7) (TST/HST) and closing with a coarsening upward sedimentation, i.e., the oxidized sandstone pointing to a mid-scale regression.

The middle part, section b (Figure 4), shows the same sedimentary pattern with i, where a fining-upward deposition prevails (the silty mudstones are overlain with a thick diatomitic package of almost equal thickness). It seems that cyclicity pertains as it is also documented in the third uppermost section c. Obviously we deal with parasequences [55] within the main depositional sequence. Section b is mostly attributable to relative small-scale sea-level changes (rise and highstand, TST to HST) and not to major structural rearrangements.

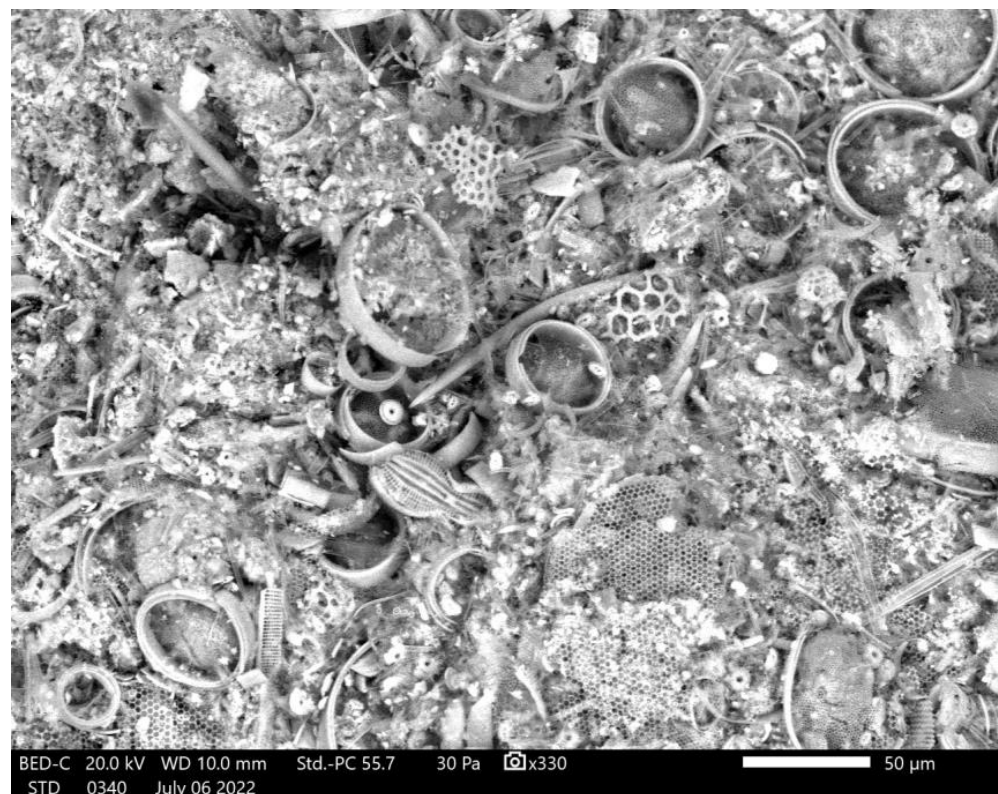


Figure 6. SEM picture of a diatomite rock fragment. Abundant, moderately preserved, marine circular diatoms (planktic forms), together with rare elongated (benthic forms) diatom frustules (A single *Diploneis bombus* can be recognized) and sponge spicules occur. Calcareous nannofossils are also to be observed (possible *Calcidiscus macintyreii*).

The top, section c, differs from the previous ones, and although it starts again at the base with silty mudstones (TST), the diatomitic package that overlies them is thinner, and a cycling of indurated sandy/silty mudstones alternations that seal the section overlies the diatomites. Oxidation traces in the top beds and the clear coarsening clearly point to the shallowing of the depositional environment. Subsequently, we interpret section c as a shallowing-upward parasequence, where the initial sea-level rise was followed by a relative fall (TST to RST). Deposition of the fine-grained facies such as diatomites represents the period of the sea-level rise where the basin reached its maximum depth. The coarse-grain package of the top could represent deposits that may be analogous to the MSC carbonate pattern that prevailed along the rim of the paleobasin by the end of the Messinian [56].

4.3. Rock-Eval Pyrolysis

Samples from a Neogene depositional succession have been characterized using RE6. Sample lithologies consist of mainly diatomites, mudstone and siltstone. According to RE6 pyrolysis the parameters regarding the thermal maturity and generation potential of the analyzed samples vary across the studied locations and across lithologies as they develop upwards. It should be noted that out of the complete set of twenty-eight (28) samples analyzed, the twenty-one (21) were found adequate for further characterization. This was linked to the mineral matrix effect [53,58,59] occurring when S2 is lower than 0.2 mg HC/g rock and the TOC content is below 0.5%wt., as well as to the oxidation of organic matter during outcrop weathering [58]. Thus, results from the RE6 pyrolysis include only the representative samples that are presented in Table 1 and plotted in the following figures.

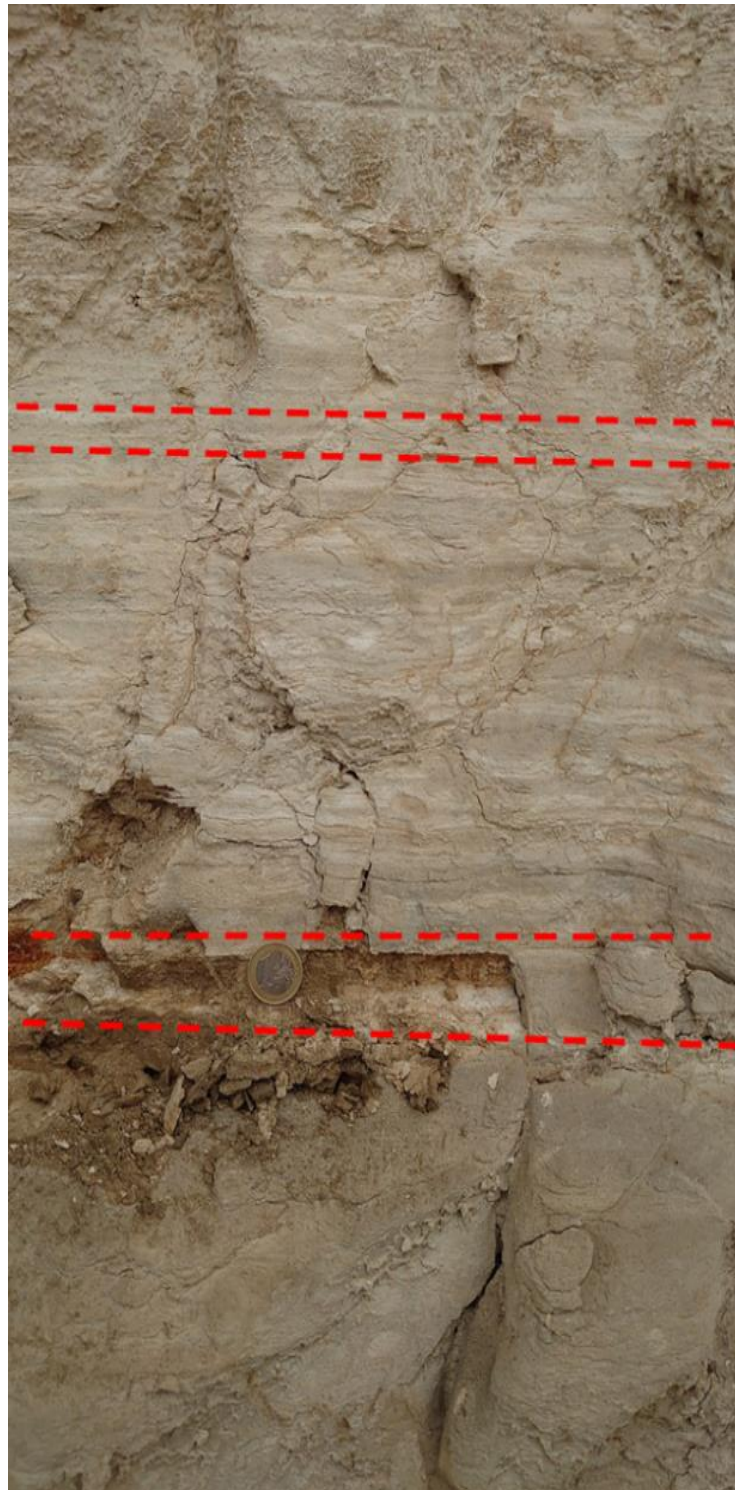


Figure 7. Fine-laminae setting framework of undisturbed, well developed diatomites. One Euro coin for scale. Light and dark laminar scale alternations are clearly to be seen (compare the upper two dotted lines in red), developed over the lower bed of a fine sandy mudstone (red dotted line below the one Euro coin). The red dotted lines below and above the coin represent the interval transition between the fine sandy mudstone and the diatomites. Red double-arrow presents the diatomites interval.

Table 1. Sample information (section, lithology) and basic Rock-Eval Pyrolysis data.

Sample/Section	Lithology	S1	S2	S3	Tmax (°C)	TOC (%wt.)	HI	OI
smpl_1i	Fine sands silts	0.4	11.51	3.77	414	3.37	342	112
smpl_1Bi	Fine sands silts	0.28	9.41	3.52	413	3.27	288	108
smpl_2i	Fine sands silts	0.02	0.51	2.11	425	0.73	70	289
smpl_3i	Fine sands silts	0.06	1.84	3.15	425	1.24	148	254
smpl_4i	Diatomites	0.33	10.27	4.14	418	3.33	308	124
smpl_5i	Diatomites	0.27	8.56	3.84	418	3.05	281	126
ex_2i	Diatomites	0.31	8.84	3.51	418	3.02	293	116
smpl_6i	Diatomites	0.27	6.35	3.13	420	2.29	277	137
smpl_7i	Diatomites	0.27	6.52	2.91	417	2.45	266	119
smpl_8i	Diatomites	0.46	8.4	3.48	412	2.77	303	126
smpl_9i	Diatomites	0.25	6.02	2.94	421	2.19	275	134
smpl_10ia	Mudstones silts	0.04	1.61	1.62	415	0.77	209	210
smpl_11ia	Mudstones silts	0.07	2.62	2.47	424	1.28	205	193
smpl_12ia	Mudstones silts	0.17	5.02	4.62	418	2.14	235	216
smpl_13ia	Diatomites	0.09	2.24	2.17	416	1.23	182	176
smpl_14ia	Diatomites	0.04	0.51	1.59	428	0.47	109	338
smpl_15ia	Diatomites	0.05	0.88	1.84	423	0.71	124	259
smpl_16ia	Diatomite muds	0.38	9.25	3.36	419	3.29	281	102
smpl_17ia	Mudstones	0.08	0.38	4.65	416	0.88	43	528
smpl_18ia	Mudstones	0.02	0.15	4.37	409	0.57	26	767
smpl_21b	Diatomites	0.02	0.28	1.73	400	0.57	49	304

Acronyms used: TOC (total organic carbon), HI (hydrogen index), OI (oxygen index), Tmax (temperature of the maximum rate of hydrocarbon generation). S1, S2, S3, HI and OI in (mg/g).

4.4. Type and Thermal Maturity of Organic Matter

Based on the RE6 pyrolysis data, kerogen was classified using the data distribution across the studied subsections. The resulting HI (mg HC/g TOC) and OI (mg CO₂/g TOC) suggest values ranging between 40–308 mg HC/g TOC and 116–340 mg CO₂/g TOC respectively for the diatomitic samples, and 26–342 mg HC/g TOC and 108–767 mg CO₂/g TOC respectively for the rest lithologies. As illustrated in Figure 8 (left diagram), the analyzed samples correspond a gas-prone type III kerogen to an inert type IV, with most diatomitic samples obtaining a solid type III response.

Overall, the level of thermal maturity documented from the evaluated samples is low. This can be seen in Figure 8 (right diagram). More specifically, Tmax reaches a maximum level of 428 °C (Figure 9) for the studied samples of all sections suggesting kerogen immaturity [60–64]

4.5. Source Rock Potential

The hydrocarbon generation potential varies across the studied subsections. Section i (lower part of the outcrop) points towards a good to excellent source-rock potential with S2 varying between 6 and 10.27 mg HC/g rock and the TOC between 2.19 and 3.33 %wt. for the diatomitic samples (Figure 10). On the contrary, section b illustrates a fair hydrocarbon-generating potential, yet with a source rock quality not as high as in section i, with 0.28 mg HC/g rock S2 and 0.57 %wt. TOC content (Figure 10).

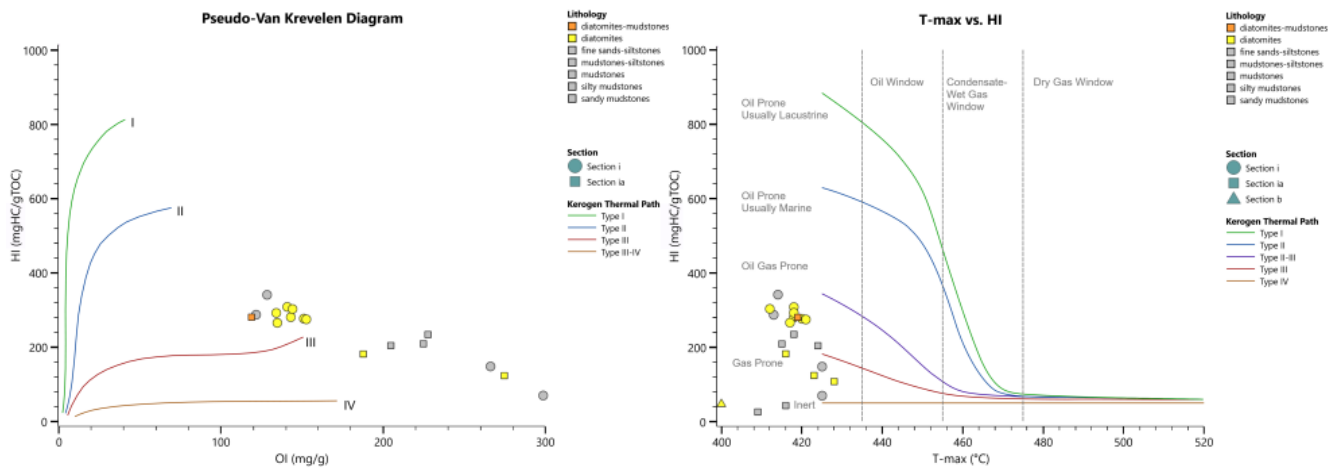


Figure 8. Pseudo Van Krevelen diagram, modified from Peters (1986), for the kerogen classification of the studied samples (left); HI (mg HC/g TOC) versus Tmax (°T) showing idealized kerogen types and thermal maturity of the samples separated by dashed lines according to Peters and Cassa (1994) and Baskin (1997) (right).

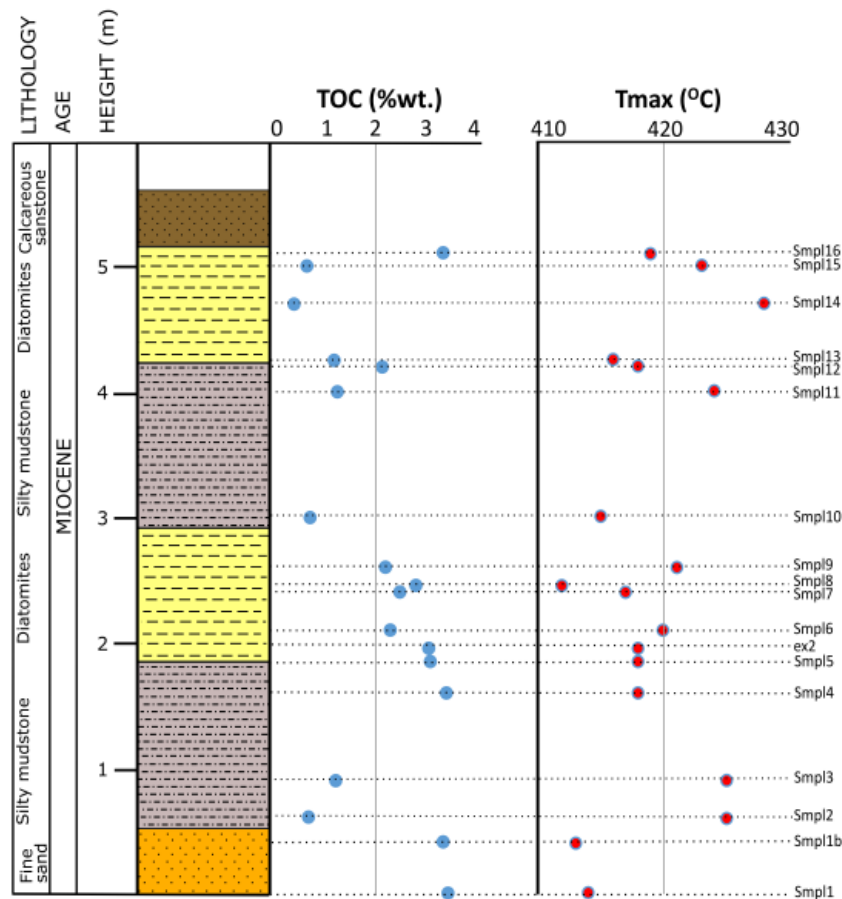


Figure 9. Lithological log of subsections i and ia (0–2.9 m height and 2.9 m-top respectively) along with the corresponding TOC (%wt.) (blue dots) and Tmax (°C) values (red dots). Note the high TOC values in the “basal” diatomites (samples 5 to 9, blue dots in the yellow interval).

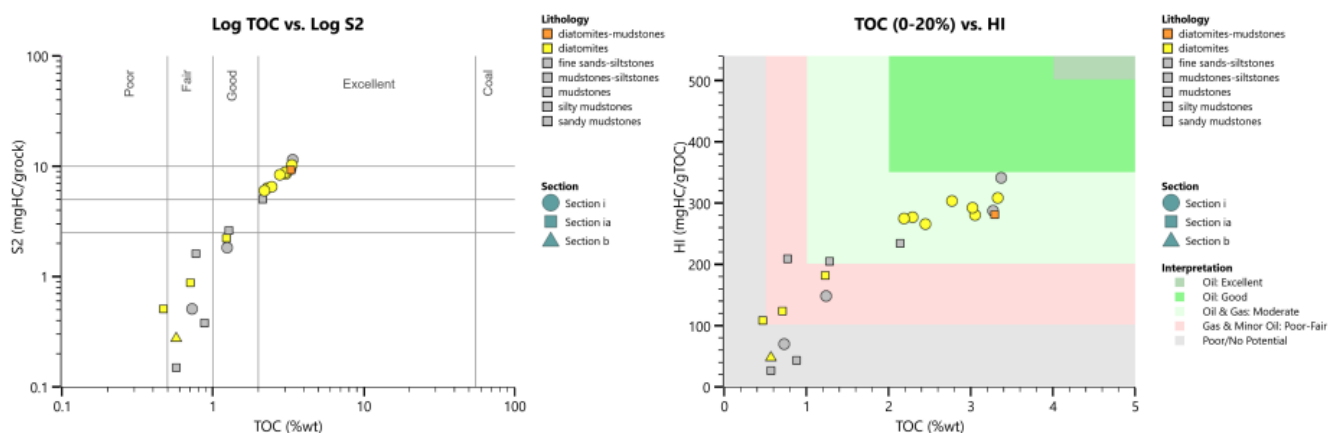


Figure 10. Logarithmic plot of TOC (%wt.) versus S2 (mg HC/g rock) illustrating the source-rock potential (left); TOC (%wt.) versus HI (mg HC/g TOC) indicating the source-rock potential and the kerogen type (right).

It is evident that diatomite samples (in yellow) obtain the highest TOC values corresponding to the highest HI values (Figure 10; right). This supports the overall frame of mainly-moderate kerogen potential, with evident differentiation between the subsections. Finally, the sum of free and potentially generated hydrocarbons (PP, S1 and S2) ranges between 0.17 and 11.91 mg HC/g rock in the studied samples. These fluctuations depict a poor-to-very good generation potential with the diatomites being clearly distinct from the rest samples.

5. Discussion

The lithostratigraphic results show that each subsection can be representative of a generally fining-upward depositional cycle, with the deeper being characterized by siliceous, fine-layered, pure diatomite packages ranging in thickness between 0.80 m (section c) and 1.5 m (section b). Coarser material closes each cycle at the top, indicating eustatic control of the deposition. Scanning Electron Microscopy gave evidence for the kind of laminites, proving that they are pure diatomites (Figure 6) with medium-to-well preservation of the frustules, since both valves are easily visible. Diagenesis seems not to have affected our material. No centrifugation was applied, trying not to bias the original depositional framework. The dominance of circular forms (centrales, diatoms) that the studied samples consist of reflects the basinal geological setting where they were accumulated. The results of this study suggest that deposition of the diatomites in western Crete is most likely connected to an early Messinian upwelling system that was active prior to the MSC onset and are in good agreement with Phase 1 of [65], (~7.2 to 6.9 Ma), where open marine conditions prevailed at the onset of the Messinian cooling.

The sequence-stratigraphic approach of the synthetic outcrop revealed that deposition occurred during the first sedimentation cycle of the Upper Miocene age. The main transgression (TST) developed as a response to tectonic movement (subsidence, basins development) and probably sea-level rise, but the four subsections studied provide evidence of a cyclicity that was controlled more by the sea-level oscillations, relevant to climate changes, than by tectonic movements. Diatomitic occurrences are connected to deepening (highstands in the transgressive regime, HST), while the coarsening of depositional material by the tops of sections represent sea-level fall and regression (RST).

The geochemical analysis of the samples along the outcrop indicated a poor (upper subsection) to very good (lower and middle subsection) hydrocarbon generation potential. Combining these results with the thickness and the geographical extending of the occurrence, it is clear that the diatomites may act as a possible gas/oil-gas prone source rock in the wider area. Further, the analysis documented high TOC values (ranging up to 3.4%wt.), a fact that makes the studied and other possible equivalent successions interesting

candidates for further investigation. A kerogen type III (with a few samples falling between II and III) is mainly recorded by the analyzed set of samples. Additionally, although all samples were proved thermally immature, their hydrocarbon potential is leaning between fair to excellent and the quality of the source rock lies around intermediate levels.

6. Summary and Conclusions

Until presently, sub-salt, mixed carbonate/siliciclastic deposits from the upper Miocene age have been investigated from central Crete and Gavdos Isls., providing poor-to-fair and/or good in a few cases for hydrocarbon generation potential [24,26,66]. Diatomites in turn have long been studied as biostratigraphic, paleoecologic indicators and as industrial materials. There are only a few, but significant works that have investigated these siliceous sedimentary rocks as potential sources for hydrocarbon generation and subsequent exploration in various basins worldwide. The latter application is examined in the present work, within the context of the eastern Mediterranean Sea and the last decades' developments for the sufficient energy supply of Europe.

In this context, and as Western Crete diatomitic deposits have not yet been geochemically investigated, this study focuses on a combined stratigraphic and geochemical analysis of a synthetic outcrop, located in the Apokoronas Neogene basin (Chania province, Greece). The studied succession is a new diatomitic occurrence of the Messinian age, and can be subdivided into four subsections. The present set of samples were investigated and analyzed by means of the RE6 pyrolysis mainly in order to gain an insight into the potential of the diatomitic beds as source rocks for hydrocarbon generation. Additionally, lithostratigraphy, SEM and sequence stratigraphy applied for a better understanding of the depositional regime. Following outcomes emerged from the current work:

1. The studied strata represent pre-evaporitic, marine deposition during the Upper Miocene.
2. Initial transgression was both tectonically and climatically controlled, while later development within the basin was mostly controlled by cyclic, eustatic sea-level oscillations. Transgressive, Highstand and Regressive System Tracks were recorded along the outcrop.
3. Medium-to-well preserved diatomites deposited in distal settings, during deepening of the basin highstands.
4. Source rock quality of the studied diatomitic deposits is proved to be around intermediate levels.
5. Hydrocarbon-generating potential lies between fair to excellent.
6. The potentially generated hydrocarbons of the analyzed diatomitic samples reach values of 10.6 mg/g.
7. Both the stratigraphical data and source rock potential illustrate a new promising case for the offshore exploration of the Crete Island and possibly for the eastern Mediterranean.

Author Contributions: Conceptualization, S.B. and D.T.; methodology, S.B., D.T., V.-I.M.; software, V.-I.M.; validation, S.B., D.T., V.-I.M. and E.M.; formal analysis, D.T. and V.-I.M.; investigation, S.B. and D.T.; resources, S.B.; data curation, D.T., S.B. and V.-I.M.; writing—original draft preparation, D.T., S.B.; writing—review and editing, D.T., S.B., V.-I.M. and E.M.; visualization, D.T., S.B., V.M.; supervision, S.B.; project administration, S.B.; funding acquisition, D.T., S.B. All authors have read and agreed to the published version of the manuscript.

Funding: This research received no external funding.

Institutional Review Board Statement: Not applicable.

Informed Consent Statement: Not applicable.

Data Availability Statement: The data used in this work is available on request.

Acknowledgments: N. Pasadakis (Institute of Geoenergy/FORTH) is acknowledged for his support throughout the project.

Conflicts of Interest: The authors declare no conflict of interest.

References

1. Zahajská, P.; Opfergelt, S.; Fritz, S.C.; Stadmark, J.; Conley, D.J. What Is Diatomite? *Quat. Res.* **2020**, *96*, 48–52. [[CrossRef](#)]
2. Pinochet, A.; Garces-Vargas, J.; Lara, C.; Olguin, F. Seasonal Variability of Upwelling off Central-Southern Chile. *Remote Sens.* **2019**, *11*, 1737. [[CrossRef](#)]
3. Moissette, P.; Bernard, C.; Martin, J. Saint Upwelling and Benthic Communities in the Messinian of Western Mediterranean. *Paleontol. I Evol.* **1992**, *24–25*, 245–254.
4. Pellegrino, L.; Dela Pierre, F.; Jordan, R.W.; Abe, K.; Mikami, Y.; Natalicchio, M.; Gennari, R.; Lozar, F.; Carnevale, G. The Upper Miocene Diatomaceous Sediments of the Northernmost Mediterranean Region: A Lamina-Scale Investigation of an Overlooked Palaeoceanographic Archive. *Sedimentology* **2020**, *67*, 3389–3421. [[CrossRef](#)]
5. Pellegrino, L.; Natalicchio, M.; Birgel, D.; Pastero, L.; Carnevale, G.; Jordan, R.W.; Peckmann, J.; Zanellato, N.; Dela Pierre, F. From Biogenic Silica and Organic Matter to Authigenic Clays and Dolomite: Insights from Messinian (Upper Miocene) Sediments of the Northern Mediterranean. *Sedimentology* **2022**, 1–33. [[CrossRef](#)]
6. Cameron, N.G. DIATOMS. In *Encyclopedia of Quaternary Science*, 2nd ed.; Elias, S.A., Mock, C.J., Eds.; Elsevier: Amsterdam, The Netherlands, 2013; pp. 522–525, ISBN 978-0-444-53642-6.
7. Flower, R.J. DIATOM METHODS | Diatomites: Their formation, distribution, and uses. In *Encyclopedia of Quaternary Science*, 2nd ed.; Elias, S.A., Mock, C.J., Eds.; Elsevier: Amsterdam, The Netherlands, 2013; pp. 501–506, ISBN 978-0-444-53642-6.
8. Stamatakis, M.; Stamatakis, G. The Use of Diatomaceous Rocks of Greek Origin As Absorbents of Olive-Oil Wasters. *Bull. Geol. Soc. Greece* **2017**, *43*, 2739. [[CrossRef](#)]
9. Stefanou, E.; Kantiranis, N.; Chatzicharalambous, K.; Mytioglaki, C.; Stamatakis, M.; Georgiadis, G. Diatomaceous Silica in Environmental Applications: A Case Study from the Lacustrine Deposit of Limnos Island, Aegean Sea, Greece. *Minerals* **2022**, *12*, 523. [[CrossRef](#)]
10. Aoyagi, K.; Omokawa, M. Neogene Diatoms as the Important Source of Petroleum in Japan. *J. Pet. Sci. Eng.* **1992**, *7*, 247–262. [[CrossRef](#)]
11. Aoyagi, K.; Omokawa, M. Diagenesis of Neogene Diatoms and Their Importance as a Source of Petroleum in Japan. *Isl. Arc* **1993**, *2*, 273–279. [[CrossRef](#)]
12. Tulan, E.; Radl, M.S.; Sachsenhofer, R.F.; Tari, G.; Witkowski, J. Hydrocarbon Source Rock Potential of Miocene Diatomaceous Sequences in Szurdokpüspöki (Hungary) and Parisdorf/Limberg (Austria). *Austrian J. Earth Sci.* **2020**, *113*, 24–42. [[CrossRef](#)]
13. Jirman, P.; Geršlová, E.; Bubík, M.; Sachsenhofer, R.F.; Bechtel, A.; Więclaw, D. Depositional Environment and Hydrocarbon Potential of the Oligocene Menilite Formation in the Western Carpathians: A Case Study from the Loučka Section (Czech Republic). *Mar. Pet. Geol.* **2019**, *107*, 334–350. [[CrossRef](#)]
14. Martizzi, P.; Chiyonobu, S.; Hibi, Y.; Yamato, H.; Arato, H. Middle–Late Miocene Paleoenvironment of the Japan Sea Inferred by Sedimentological and Geochemical Characterization of Coeval Sedimentary Rocks. *Mar. Pet. Geol.* **2021**, *128*, 105059. [[CrossRef](#)]
15. Mayer, J.; Rupprecht, B.; Sachsenhofer, R.; Tari, G.; Bechtel, A.; Coric, S.; Siedl, W.; Kosi, W.; Floodpage, J. Source Potential and Depositional Environment of Oligocene and Miocene Rocks Offshore Bulgaria. *Geol. Soc. Lond. Spec. Publ.* **2017**, *464*, 307–328. [[CrossRef](#)]
16. Sachsenhofer, R.F.; Popov, S.V.; Coric, S.; Mayer, J.; Misch, D.; Morton, M.T.; Pupp, M.; Rauball, J.; Tari, G. Paratethyan petroleum source rocks: An overview. *J. Pet. Geol.* **2018**, *41*, 219–245. [[CrossRef](#)]
17. Sachsenhofer, R.F.; Popov, S.V.; Bechtel, A.; Coric, S.; Francu, J.; Gratzner, R.; Grunert, P.; Kotarba, M.; Mayer, J.; Pupp, M.; et al. Oligocene and Lower Miocene Source Rocks in the Paratethys: Palaeogeographical and Stratigraphic Controls. *Geol. Soc. Spec. Publ.* **2018**, *464*, 267–306. [[CrossRef](#)]
18. Freudenthal, T. Stratigraphy of Neogene Deposits in the Khania Province, Crete, with Special Reference to Foraminifera of the Family Planorbulinidae and the Genus Heterostegina. *Utr. Micropaleontol. Bull.* **1969**, *1*, 1–208.
19. Zachariasse, W.J.; Lourens, L.J. About the Age and Depositional Depth of the Sediments with Reported Bipedal Footprints at Trachilos (NW Crete, Greece). *Sci. Rep.* **2022**, *12*, 18471. [[CrossRef](#)] [[PubMed](#)]
20. Keupp, H.; Bellas, S. Neogene Development of the Sedimentary Basins of NW Crete Island, Chania Prefecture, South Aegean Arc System (Greece). *Berl. Geowiss. Abh.* **2000**, *34*, 3–117.
21. Zachariasse, W.J.; Kontakiotis, G.; Lourens, L.J.; Antonarakou, A. The Messinian of Agios Myron (Crete, Greece): A Key to Better Understanding of Diatomite Formation on Gavdos (South of Crete). *Palaeogeogr. Palaeoclimatol. Palaeoecol.* **2021**, *581*, 110633. [[CrossRef](#)]
22. Drinia, H.; Antonarakou, A.; Tsaparas, N.; Dermitzakis, M.D.; Kontakiotis, G. Foraminiferal record of environmental changes: Preevaporitic diatomaceous sediments from Gavdos island, southern Greece. *Bull. Geol. Soc. Greece* **2018**, *36*, 782. [[CrossRef](#)]
23. Frydas, D. Siliceous Phytoplankton Assemblages and Biostratigraphy of the Pre-Evaporite Messinian Diatomites on Gavdos Island, Greece. *Rev. Micropaleontol.* **2006**, *49*, 86–96. [[CrossRef](#)]
24. Pyliotis, I.; Hamilaki, E.; Pasadakis, N.; Manoutsoglou, E. Comparative Evaluation of Rock-Eval and Elemental Analysis to Determine Organic Carbon Content in Sediment Samples. *Bull. Geol. Soc. Greece* **2013**, *47*, 862–870. [[CrossRef](#)]
25. Pellegrino, L.; Dela Pierre, F.; Natalicchio, M.; Carnevale, G. The Messinian Diatomite Deposition in the Mediterranean Region and Its Relationships to the Global Silica Cycle. *Earth Sci. Rev.* **2018**, *178*, 154–176. [[CrossRef](#)]

26. Maravelis, A.G.; Kontakiotis, G.; Bellas, S.; Antonarakou, A.; Botziolis, C.; Janjuhah, H.T.; Makri, P.; Moissette, P.; Cornée, J.J.; Pasadakis, N.; et al. Organic Geochemical Signatures of the Upper Miocene (Tortonian—Messinian) Sedimentary Succession Onshore Crete Island, Greece: Implications for Hydrocarbon Prospectivity. *J. Mar. Sci. Eng.* **2022**, *10*, 1323. [[CrossRef](#)]
27. Telemenis, D.; Makridou, Z.; Bellas, S. New Evidence of Diatomitic Occurrences in Western Crete, Greece; A Preliminary Stratigraphic and Geochemical Approach and Its Implications. *Bull. Geol. Soc. Greece* **2022**, *9*, 81–82.
28. Decentralized Administration of Crete—IT and Communications Directorate Geological Map of Crete. Available online: <https://www.apdkritis.gov.gr/> (accessed on 13 December 2022).
29. McKenzie, D. The Plate Tectonics of the Mediterranean Region. *Nature* **1970**, *226*, 239–243. [[CrossRef](#)] [[PubMed](#)]
30. Makris, J. The Crust and Upper Mantle of Aegean Region from Deep Seismic Soundings. *Tectonophysics* **1978**, *46*, 269–284. [[CrossRef](#)]
31. Le Pichon, X.; Angelier, J. The hellenic arc and trench system: A key to the neotectonic evolution of the eastern mediterranean area. *Tectonophysics* **1979**, *60*, 1–42. [[CrossRef](#)]
32. Angelier, J.; Lybéris, N.; Le Pichon, X.; Barrier, E.; Huchon, P. The Tectonic Development of the Hellenic Arc and the Sea of Crete: A Synthesis. *Tectonophysics* **1982**, *86*, 159–163, 165, 167–196. [[CrossRef](#)]
33. van Hinsbergen, D.J.J.; Meulenkamp, J.E. Neogene Supradetachment Basin Development on Crete (Greece) during Exhumation of the South Aegean Core Complex. *Basin Res.* **2006**, *18*, 103–124. [[CrossRef](#)]
34. Kopf, A. The Mediterranean Ridge: A Mass Balance across the Fastest Growing Accretionary Complex on Earth. *J. Geophys. Res.* **2003**, *108*, 2372. [[CrossRef](#)]
35. Le Quellec, P.; Mascle, J.; Got, H.; Vittori, J. Seismic Structure of Southwestern Peloponnesus Continental Margin1. *AAPG Bull.* **1980**, *64*, 242–263. [[CrossRef](#)]
36. Jongsma, D. Pliny and Strabo Trenches, South of the Hellenic Arc. *Geol. Soc. Am. Bull.* **1977**, *88*, 797–805. [[CrossRef](#)]
37. Peters, J.M.; Troelstra, S.R.; van Harten, D. Late Neogene and Quaternary Vertical Movements in Eastern Crete and Their Regional Significance. *J. Geol. Soc. London.* **1985**, *142*, 501–513. [[CrossRef](#)]
38. Sakellariou, D.; Tsampouraki-Kraounaki, K. Chapter 14—Plio-Quaternary extension and Strike-Slip tectonics in the Aegean. In *Transform Plate Boundaries and Fracture Zones*; Duarte, J.C., Ed.; Elsevier: Amsterdam, The Netherlands, 2019; pp. 339–374, ISBN 978-0-12-812064-4.
39. Lazos, I.; Sboras, S.; Chousianitis, K.; Kondopoulou, D.; Pikridas, C.; Bitharis, S.; Pavlides, S. Temporal Evolution of Crustal Rotation in the Aegean Region Based on Primary Geodetically-Derived Results and Palaeomagnetism. *Acta Geod. Geophys.* **2022**, *57*, 317–334. [[CrossRef](#)]
40. Sboras, S.; Lazos, I.; Bitharis, S.; Pikridas, C.; Galanakis, D.; Fotiou, A.; Chatzipetros, A.; Pavlides, S. Source Modelling and Stress Transfer Scenarios of the October 30, 2020 Samos Earthquake: Seismotectonic Implications. *Turk. J. Earth Sci.* **2021**, *30*, 699–717. [[CrossRef](#)]
41. Meulenkamp, J.E. Field Guide to the Neogene of Crete. *Publ. Dep. Geol. Paleontol. Univ. Athens* **1979**, *32*, 1–32.
42. Meulenkamp, J.E.; Wortel, M.J.R.; Van Wamel, W.A.; Spakman, W.; Strating, E.H. On the Hellenic Subduction Zone and the Geodynamic Evolution of Crete since the Late Middle Miocene. *Tectonophysics* **1988**, *146*, 203–215. [[CrossRef](#)]
43. Meulenkamp, J.E.; Van Der Zwaan, G.J.; Van Wamel, W.A. On Late Miocene to Recent Vertical Motions in the Cretan Segment of the Hellenic Arc. *Tectonophysics* **1994**, *234*, 53–72. [[CrossRef](#)]
44. Zachariasse, W.J.; van Hinsbergen, D.J.J.; Fortuin, A.R. Formation and Fragmentation of a Late Miocene Supradetachment Basin in Central Crete: Implications for Exhumation Mechanisms of High-Pressure Rocks in the Aegean Forearc. *Basin Res.* **2011**, *23*, 678–701. [[CrossRef](#)]
45. Mouslopoulou, V.; Begg, J.; Nicol, A.; Oncken, O.; Prior, C. Formation of Late Quaternary Paleoshorelines in Crete, Eastern Mediterranean. *Earth Planet. Sci. Lett.* **2015**, *431*, 294–307. [[CrossRef](#)]
46. Ott, R.F.; Wegmann, K.W.; Gallen, S.F.; Pazzaglia, F.J.; Brandon, M.T.; Ueda, K.; Fassoulas, C. Reassessing Eastern Mediterranean Tectonics and Earthquake Hazard from the 365 CE Earthquake. *AGU Adv.* **2021**, *2*, e2020AV000315. [[CrossRef](#)]
47. Frydas, D.; Keupp, H. Biostratigraphical Results in Late Neogene Deposits of NW Crete, Greece, Based on Calcareous Nannofossils. *Berl. geowiss. Abh.* **1996**, *E18*, 169–189.
48. Kontopoulos, N.; Zelilidis, A.; Frydas, D. Late Neogene Sedimentary and Tectonostratigraphic Evolution of Northwestern Crete Island, Greece. *Neues Jahrb. Fur Geol. Und Palaontologie—Abhandlungen* **1996**, *202*, 287–311. [[CrossRef](#)]
49. Zachariasse, W. Planktonic Foraminiferal Biostratigraphy of the Late Neogene of Crete (Greece). *Utr. Micropaleontol. Bull.* **1975**, *11*, 1–171.
50. Lafargue, E.; Marquis, F.; Pillot, D. Rock-Eval 6 Applications in Hydrocarbon Exploration, Production, and Soil Contamination Studies. *Oil Gas Sci. Technol.* **1998**, *53*, 421–437. [[CrossRef](#)]
51. Behar, F.; Beaumont, V.; De, H.L. Technologie Rock-Eval 6: Performances et Développements. *Oil Gas Sci. Technol.* **2001**, *56*, 111–134. [[CrossRef](#)]
52. Disnar, J.R.; Guillet, B.; Keravis, D.; Di-Giovanni, C.; Sebag, D. Soil Organic Matter (SOM) Characterization by Rock-Eval Pyrolysis: Scope and Limitations. *Org. Geochem.* **2003**, *34*, 327–343. [[CrossRef](#)]
53. Yang, S.; Horsfield, B. Critical Review of the Uncertainty of Tmax in Revealing the Thermal Maturity of Organic Matter in Sedimentary Rocks. *Int. J. Coal Geol.* **2020**, *225*, 103500. [[CrossRef](#)]

54. Catuneanu, O. Sequence stratigraphy: Guidelines for a standard methodology. In *Stratigraphy & Timescales*; Academic Press: Cambridge, MA, USA, 2017; Volume 2, pp. 1–57.
55. Clark, M.S. Sequence stratigraphy of an interbedded biogenic-clastic reservoir, Belridge diatomite at lost hills field, San Joaquin basin, California. *Geol. Soc. Am. Abstr. Programs* **2001**, *33*, 35.
56. Goldstein, R.H.; Franseen, E.K. Carbonate Play Models from Miocene Outcrops, Western Mediterranean: Part 2-Stratigraphic and Diagenetic Plays. AAPG Geoscience Technology Workshop. *AAPG* **2019**. [[CrossRef](#)]
57. Behl, R.J. Monterey Formation Overview and Context for New Research. *AAPG* **2022**. [[CrossRef](#)]
58. Peters, K.E. Guidelines for Evaluating Petroleum Source Rock Using Programmed Pyrolysis. *AAPG Bull.* **1986**, *70*, 3.
59. Reynolds, J.G.; Burnham, A.K. Comparison of Kinetic Analysis of Source Rocks and Kerogen Concentrates. *Org. Geochem.* **1995**, *23*, 11–19. [[CrossRef](#)]
60. Peters, K.E.; Cassa, M.R. Applied source rock geochemistry. In *The Petroleum System: From Source to Trap*; Magoon, L.B., Dow, W.G., Eds.; AAPG Memoir: Boulder, CO, USA; Tulsa, OK, USA, 1994; Volume 60; pp. 93–120.
61. Espitalie, J.; Marquis, F.; Barsony, I. Geochemical logging. In *Analytical Pyrolysis—Technics and applications*; Voorhees, K.J., Ed.; Butterworth: Boston, MA, USA, 1984; pp. 276–304. [[CrossRef](#)]
62. Baskin, D. Atomic H/C Ratio of Kerogen as an Estimate of Thermal Maturity and Organic Matter Conversion. *AAPG Bull.* **1997**, *81*, 1437–1450. [[CrossRef](#)]
63. Killips, S.; Killips, V. *An Introduction to Organic Geochemistry*; Wiley: Hoboken, NJ, USA, 2013; pp. 1–408.
64. Dellisanti, F.; Pini, G.A.; Baudin, F. Use of T Max as a Thermal Maturity Indicator in Orogenic Successions and Comparison with Clay Mineral Evolution. *Clay Miner.* **2010**, *45*, 115–130. [[CrossRef](#)]
65. Kontakiotis, G.; Butiseacă, G.A.; Antonarakou, A.; Agiadi, K.; Zarkogiannis, S.D.; Krsnik, E.; Besiou, E.; Zachariasse, W.J.; Lourens, L.; Thivaïou, D.; et al. Hypersalinity Accompanies Tectonic Restriction in the Eastern Mediterranean Prior to the Messinian Salinity Crisis. *Palaeogeogr. Palaeoclimatol. Palaeoecol.* **2022**, *592*, 110903. [[CrossRef](#)]
66. Kontakiotis, G.; Karakitsios, V.; Cornée, J.-J.; Moissette, P.; Zarkogiannis, S.D.; Pasadakis, N.; Koskeridou, E.; Manoutsoglou, E.; Drinia, H.; Antonarakou, A. Preliminary Results Based on Geochemical Sedimentary Constraints on the Hydrocarbon Potential and Depositional Environment of a Messinian Sub-Salt Mixed Siliciclastic-Carbonate Succession Onshore Crete (Plouti Section, Eastern Mediterranean). *Mediterr. Geosci. Rev.* **2020**, *2*, 247–265. [[CrossRef](#)]

Disclaimer/Publisher’s Note: The statements, opinions and data contained in all publications are solely those of the individual author(s) and contributor(s) and not of MDPI and/or the editor(s). MDPI and/or the editor(s) disclaim responsibility for any injury to people or property resulting from any ideas, methods, instructions or products referred to in the content.